Detection of downy mildew of opium poppy using high-resolution multi-spectral and thermal imagery acquired with an unmanned aerial vehicle

R. Calderón, M. Montes-Borrego, B. B. Landa, J. A. Navas-Cortés & P. J. Zarco-Tejada

Precision Agriculture
An International Journal on Advances in Precision Agriculture

ISSN 1385-2256
Volume 15
Number 6

Precision Agric (2014) 15:639-661
DOI 10.1007/s11119-014-9360-y

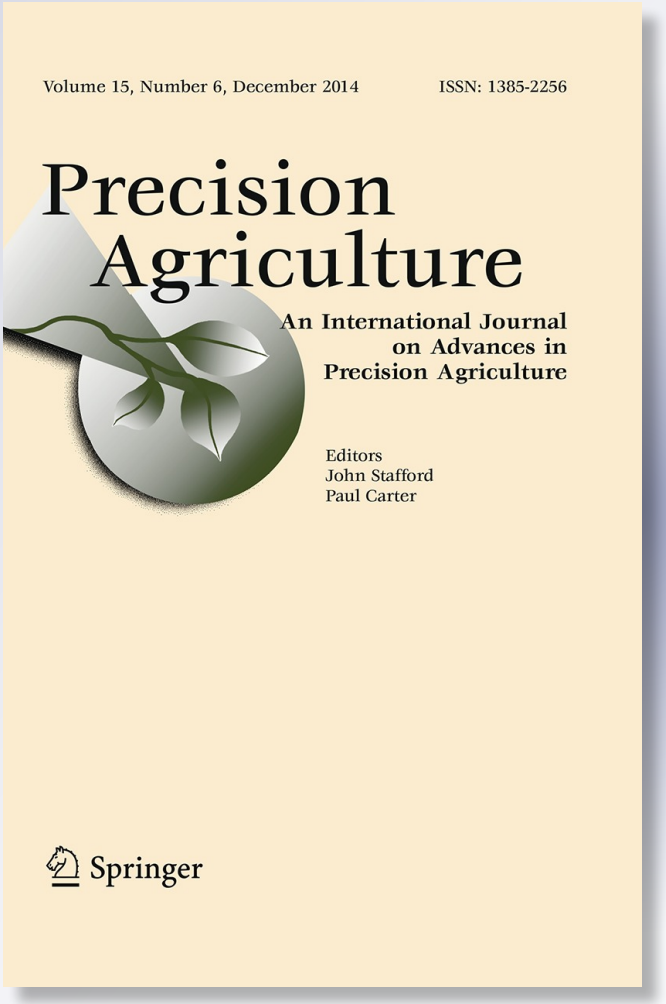

Springer

Precision Agric (2014) 15:639–661
DOI 10.1007/s11119-014-9360-y

Detection of downy mildew of opium poppy using high-resolution multi-spectral and thermal imagery acquired with an unmanned aerial vehicle

R. Calderón · M. Montes-Borrego · B. B. Landa · J. A. Navas-Cortés · P. J. Zarco-Tejada

Published online: 23 April 2014

Abstract Downy mildew (DM) caused by the biotrophic obligate oomycete *Peronospora arborescens* (Berk.) is one of the most economically limiting diseases of opium poppy (*Papaver somniferum* L.) worldwide. The first symptoms appear as small chlorotic leaf lesions, which can evolve to curled and thickened tissues that become deformed and necrotic as the disease develops. The present study explored the use of high-resolution thermal and multi-spectral imagery as an indicator of DM infection. Work was conducted in two opium poppy field plots artificially infected by *P. arborescens*. Airborne thermal and multi-spectral imagery were acquired at 200 mm resolution on three dates in spring of 2009 using an unmanned aerial vehicle (UAV). Leaf reflectance and transmittance spectra of DM asymptomatic and symptomatic opium poppy leaves were measured using an integrating sphere. Simulation work was conducted with the coupled PROSPECT + SAILH radiative transfer model to assess the effects of the variability found in an opium poppy plot developing a DM epidemic on the normalized difference vegetation index (NDVI) and the green/red index (R_{550}/R_{670}) calculated from the multi-spectral imagery. The airborne flights enabled DM detection by using image-derived canopy temperature (Tc) normalized by air temperature (Tc − Ta) and the green/red index (R_{550}/R_{670}). T_{min} for each grid unit was calculated to estimate pure-vegetation temperature removing background and soil effects. T_{min} − Ta and R_{550}/R_{670} were assessed as a function of aggregated NDVI clusters to compare asymptomatic and symptomatic plants normalized by similar growth levels. Results demonstrated that Tc − Ta and the R_{550}/R_{670} index were related to physiological stress caused by DM infection. In addition, T_{min} − Ta was found to decrease as the NDVI increased and symptomatic plants reached significantly higher ($P < 0.05$) temperatures for an NDVI $\geq$0.6. The R_{550}/R_{670} index was positively correlated with the NDVI, showing significantly higher values ($P < 0.05$) in symptomatic plants with an NDVI $\geq$0.5. These results demonstrate the feasibility of detecting *P.*

R. Calderón · M. Montes-Borrego · B. B. Landa · J. A. Navas-Cortés · P. J. Zarco-Tejada (✉)
Instituto de Agricultura Sostenible (IAS), Consejo Superior de Investigaciones Científicas (CSIC), Cordoba, Spain
e-mail: pzarco@ias.csic.es

arborescens infection in opium poppy plants using high-resolution thermal and multi-spectral imagery acquired with an UAV.

Keywords Thermal · Multi-spectral · High resolution · UAV · Opium poppy · Downy mildew · *Peronospora arborescens*

Introduction

Downy mildew (DM) of opium poppy (*Papaver somniferum* L.), caused either by the biotrophic obligate oomycete *Peronospora arborescens* (Berk.) (Landa et al. 2005) or *P. cristata* (Scott et al. 2004), is one of the most economically restrictive diseases for this crop worldwide (Yossifovitch 1929; Khristov 1943; Kapoor 1995; Landa et al. 2007). Opium poppy is a strategic crop for the pharmaceutical industry because it is the only source of the alkaloid drugs morphine, codeine and thebaine.

In Spain, the fourth largest global producer, DM is caused by *P. arborescens* (Landa et al. 2005). The severity of *P. arborescens* attacks strongly depends on the duration of optimal environmental conditions for disease development and pathogen sporulation, that is, high relative humidity and moderate temperature (Weltzien 1981; Montes-Borrego et al. 2009a). Over the last few years, the incidence and severity of DM attacks have steadily increased. This is mainly due to the expansion of the crop to new cooler and irrigated areas in central Spain in order to improve harvest yields (Landa et al. 2007).

DM pathogens can cause local or systemic infections in plants. Such infections can evolve producing large numbers of short-lived sporangia and/or oospores, which are thought to be dispersed from a few hundred meters up to hundreds of kilometers by air currents in viable conditions. According to research findings, the main sources of primary inoculum are diseased plant parts carrying sporangia and oospores or soil harboring oospores (Navas-Cortés et al. 2009; Montes-Borrego et al. 2011). The sporangia of *P. arborescens* formed on infected plants are effective as inoculum to produce secondary local infections, which trigger a sequence of different symptoms. After infecting the leaf, the pathogen colonizes the mesophyll, forming haustoria in parenchymatic cells and causing the first symptoms: small, chlorotic to light-yellow leaf lesions with intense sporulation on the abaxial surface. These initial symptoms can evolve to a second stage in which affected tissues are irregularly shaped, curled and thickened and become deformed and necrotic as the disease develops. Lesions expand in size and often coalesce, eventually giving rise to large necrotic areas in leaves or death of entire leaves (Populer 1981; Landa et al. 2005). Moreover, in wet weather or under high relative humidity conditions, a dense felt of sporangiophores with sporangia is produced on the abaxial leaf surface and occasionally on the adaxial surface (Landa et al. 2005).

Infection by DM pathogens results in changes in the metabolic processes of plant tissues including shifts in respiration, photosynthesis and transpiration (Ingram 1981). Lindenthal et al. (2005) conducted laboratory studies using digital infrared thermography. They reported an increase in transpiration rate and a decrease in leaf temperature at early stages of infection of cucumber leaves by *Pseudoperonospora cubensis*; yet, the opposite occurred with further DM development, where the authors recorded the appearance of chlorotic and necrotic tissue, increased water loss and the inability of plant tissue to regulate stomatal opening. Oerke et al. (2006) used a similar experimental approach to explore this pathosystem. Similarly, they reported that the highest temperature difference

within a leaf increased during pathogenesis with the formation of necrotic tissue. They found that this was related to disease severity and that it could be used to discriminate between healthy and infected areas in thermograms, even before the appearance of visible DM symptoms.

Use of remote sensing methods for crop management (e.g. disease detection) requires high spatial and spectral resolution. Current satellite-based imagery has limited application in crop management due to the low spatial and spectral resolutions provided and the long revisit periods. High spatial resolution imagery acquired in the visible and near infrared regions is relatively feasible with current airborne and satellite sensors. By contrast, thermal imaging is still limited to medium-resolution sensors due to the technical limitations of micro-bolometer technology (Berni et al. 2009a). As an example, the Landsat Data Continuity Mission launched in February 2013 delivers two thermal infrared bands at 100 m resolution. Although it is useful for certain global monitoring studies, the low resolution of the thermal bands is a clear limitation for precision agriculture methods. Alternatives based on manned airborne platforms have demonstrated capabilities for vegetation condition monitoring due to the high spatial resolution used (0.5–2 m pixel sizes). However, their use is limited because of their high operational costs (Berni et al. 2009b). Remote sensors on board unmanned aerial vehicle (UAV) platforms provide submeter spatial resolution (Herwitz et al. 2004; Sugiura et al. 2005; Berni et al. 2009b). This allows retrieving of pure canopy temperature and spectral indices, thus minimizing background and shadow effects.

In previous studies, remote sensing has been used for the detection of illegal narcotics crops such as opium poppy in Central Asia. Zaitseva et al. (1997) showed that the brightness spectra of particular phyto-elements of opium poppy have specific properties that are characteristic of certain vegetative stages and can successfully be used to detect poppy crops and distinguish them from other crops such as wheat. The weighted difference vegetation index has also proven to be useful in discriminating between winter wheat and opium poppy crops, considering that the NDVI is limited due to its saturation when crop density or LAI is high (Srinivas et al. 2004).

Remote sensing has also been used to detect, monitor and quantify a wide variety of diseases in different crops. Comprehensive reviews are available on the use of remote sensing to detect plant diseases (e.g. Nilsson 1995; West et al. 2003; Sankaran et al. 2010; Barton 2012). Most of these studies have focused on powdery mildew and leaf rust diseases in cereals and few studies have dealt with DM pathogens. In greenhouse experiments, *Plasmopara viticola* caused a pre-symptomatic increase in leaf temperature at the site of infection in irrigated grapevine, whereas drought-stressed plants showed a localized drop in temperature 2–3 days before the typical symptoms of DM appeared (Stoll et al. 2008a). In another study, spatial and temporal analysis of leaf temperature was successfully used to distinguish between healthy and infected leaves irrespective of their water status (Stoll et al. 2008b). However, under field conditions, cucumber plants infected by *P. cubensis* exhibited differential changes in leaf temperature and chlorophyll content only at high levels of DM infection (Oerke et al. 2005).

The main objective of this research was to evaluate the use of high-resolution canopy temperature and multi-spectral indices related to chlorophyll content and canopy structure as indicators of DM infection. The hypothesis under study was that thermal imagery, the green/red ratio (R_{550}/R_{670}) and the NDVI structural index acquired from airborne imagery are sensitive to physiological changes induced by the infection and colonization of opium poppy by *P. arborescens*.

Materials and methods

Experimental site description

The experimental area was located in Cordoba, in southern Spain, a region of Mediterranean climate characterized by warm and dry summers and cool and wet winters, with an average annual rainfall exceeding 550 mm. Two experiments were conducted in two fields (45 × 20 m) at Alameda del Obispo Research Station (37°51′21″ N, 4°48′03″W) to account for differences in sources of *P. arborescens* primary inoculum. These fields had never been sown with opium poppy before and no commercial opium poppy crops were being grown within a radius of 50 km. An opium poppy certified seed lot of cv. Nigrum was used. The opium poppy seeds were sown in February 2009 at a spacing of 80 mm × 0.50 m (ca. 22 500 plants per plot with a plant density of approximately 25 plants per m^2). The plots were sown with a precision seeder Hege 80 (Wintersteiger Gmbh, Ried, Austria) and irrigated by sprinkler irrigation as needed.

Peronospora arborescens inoculum and disease assessment

In Plot 1, the inoculum source of the disease was soil obtained from an opium poppy field highly infected by downy mildew at Ecija (Seville province, Spain). The soil contained debris of opium poppy leaves with oospores of *P. arborescens* (Montes-Borrego et al. 2009b). Before sowing in 2009, 200 kg of infested soil were sieved and thoroughly mixed with the uppermost 100 mm soil layer covering an area of 1 m^2 of the plot. This source of inoculum was placed in two different areas of the plot at a distance of 15 and 30 m from the central line running along the length of the plot.

In Plot 2, the inoculum source was opium poppy plants artificially inoculated with *P. arborescens* showing profuse sporulation on the abaxial surface of the leaves. Three plants were planted with the following arrangement: row 4, 4 m from the edge; row 36, 4 m from the edge; and row 20, 10 m from the edge, forming a triangle. To obtain infected plants for use as a source of inoculum, four-week-old opium poppy plants with 6–8 true leaves were drop-inoculated with a 25-µl-drop containing 10^4 sporangia of *P. arborescens* placed at the junction of each leaf petiole with the stem. After inoculation, plants were placed inside a moistened transparent polyethylene bag to provide a confined environment with high relative humidity (RH). Inoculated and control plants were incubated at 17 ± 1 °C in the dark for 24 h and at the same temperature under a 10-h photoperiod of fluorescent light and 70/90 % RH thereafter. Plants were removed from the bags three days after inoculation and kept in the conditions referred to above until sporulation (15 days approximately).

DM incidence was assessed by visually inspecting every plant for disease symptoms and the signs described above in the plots at approximately 4-week intervals from February to June. Plant growth stages evaluated included rosette, shooting, flowering and capsule formation.

Leaf-level measurements

Reflectance and transmittance measurements of opium poppy leaves were taken from 20 asymptomatic leaves and 20 leaves showing a range of severity of DM symptoms (initial small chlorotic to light-yellow leaf lesions to complete chlorosis of the entire leaf). This was done with a Li-Cor 1800-12 Integrating Sphere (Li-Cor, Inc., Lincoln, NE, USA),

coupled by a 200-μm diameter single mode fiber to a spectrometer (Ocean Optics Inc., Dunedin, FL, USA) with a 2048 element detector array, 0.5 nm sampling interval and 7.5 nm spectral resolution in the 350–1 000 nm range. Single leaf reflectance (ρ) and transmittance (τ) values were acquired as described in Zarco-Tejada et al. (2005). As an example of spectra measured with this methodology, Fig. 1 shows opium poppy leaf reflectance and transmittance spectra measurements taken from a DM asymptomatic (Fig. 1a) and a DM symptomatic leaf (Fig. 1b) and 5 leaf reflectance measurements from leaves showing a gradient in DM severity between asymptomatic and severely affected leaves (Fig. 1c). The leaf optical measurements taken with the Li-Cor 1800-12 integrating sphere used in this study were used to detect spectral differences between DM asymptomatic and symptomatic leaves.

Airborne imagery and remote sensing indices

Imagery was acquired from both experimental plots on three dates (21 April, 24 April and 4 May 2009) using multi-spectral and thermal cameras. Multi-spectral and thermal images were always acquired at the same time (i.e. 11.00 and 14.00 GMT, respectively) to minimize differences due to sun angle effects. Flights were conducted with an UAV operated by the Laboratory for Research Methods in Quantitative Remote Sensing (Quantalab, IAS-CSIC, Spain) (Zarco-Tejada et al. 2008; Berni et al. 2009b; Zarco-Tejada et al. 2012). The UAV platform operated in this study consisted of a 2-m wingspan fixed-wing platform capable of 1-h flight duration at 5.8 kg take-off weight (MX-SIGHT, UAV Services and Systems, Germany). The UAV was controlled by an autopilot system (AP04, UAV Navigation, Madrid, Spain) that provided autonomous flight based on waypoints programmed during the mission planning.

The multi-spectral sensor was a 3-band multi-spectral camera (ADC Lite, Tetracam, Inc., California, USA) flown 200 m above ground level (AGL). The camera had a single CMOS sensor that was designed to capture images at 550, 670 and 800 nm wavelengths. Image resolution was 2 048 × 1 536 pixels with 10-bit radiometric resolution and an optical focal length of 8.5 mm. Atmospheric correction and radiometric calibration methods were applied to the imagery to calculate the spectral reflectance. The multi-spectral images were radiometrically calibrated with a uniform light source system (an integrating sphere, CSTM-USS-2000C Uniform Source System, LabSphere, NH, USA) at four levels of illumination and six integration times. Atmospheric correction was performed with the SMARTS simulation model (Gueymard, 1995; 2001) using aerosol optical depth measured at 500 nm with a Micro-Tops II sunphotometer (Solar LIGHT Co., Philadelphia, PA, USA) in the experimental areas at the time of the flights (as in Berni et al. 2009a, b; Suárez et al. 2010 and Zarco-Tejada et al. 2012).

Mean radiance and reflectance spectra calculated for the three spectral bands (B1 centered at 550 nm; B2 at 670 nm; and B3 at 800 nm) obtained by the multi-spectral camera were used to calculate the Normalized Difference Vegetation Index, $NDVI = (R_{800} - R_{670})/(R_{800} + R_{670})$ (Rouse et al. 1974) and the green/red ratio, R_{550}/R_{670} (this study).

The 640 × 480 pixel thermal camera used in this study (MIRICLE 307, Thermoteknix Systems Ltd, Cambridge, UK) was flown at 100 m AGL. It was a 14.25 mm f1.3 lens camera connected to a computer via a USB 2.0 protocol (see Berni et al. 2009a for further details). Radiometric calibration was performed in the laboratory using blackbodies at varying target and ambient temperatures to develop radiometric calibration algorithms along with an internal calibration for non-uniformity correction (NUC). Local atmospheric

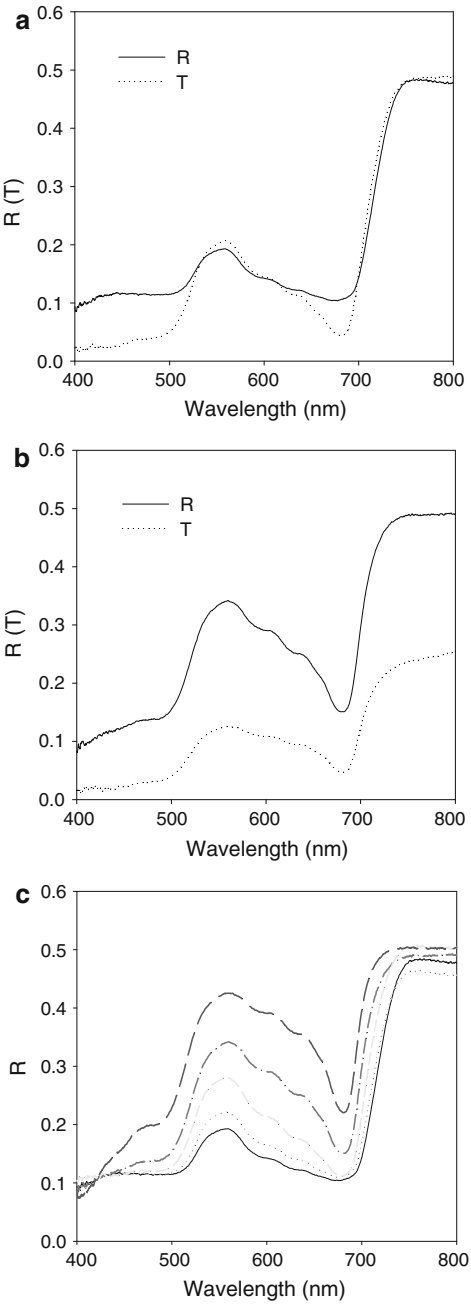

Fig. 1 Sample leaf reflectance (R) and transmittance (T) measured in DM asymptomatic (**a**) and symptomatic (**b**) *Papaver somniferum* L. leaves with the integrating sphere and protocol described in Zarco-Tejada et al. (2005). The *bottom* plot (**c**) shows 5 leaf reflectance measurements for opium poppy leaves ranging from asymptomatic leaf reflectance to 4 reflectances corresponding to gradual states of DM symptom severity in leaves

conditions were determined using a portable weather station (Model WXT510, Vaisala, Finland) by measuring air temperature, relative humidity and barometric pressure at the time of each flight.

Multi-spectral (Fig. 2a, b) and thermal images (Figs. 2c, d, 3a) were acquired at 200 mm pixel resolution. A uniform grid (Fig. 3b) was created with the same dimensions of each plot so that each cell of the grid measured the exact planting distance (80 mm × 500 mm). Each cell was used to retrieve the thermal and multi-spectral data from its corresponding area of the image (Fig. 3c). In particular, the grid for both multi-spectral and thermal images on each flight date was generated and the average, minimum and maximum temperatures (from the thermal imagery), and the average, minimum and maximum NDVI and R_{550}/R_{670} indices (from the multi-spectral imagery) were extracted for each cell, assessing the relationship with DM incidence. Soil pixels showing higher temperature values can be observed in Fig. 4, illustrating the average (T_{avg}), minimum (T_{min}) and maximum (T_{max}) temperature maps. The maps of the minimum temperature per cell intended to reduce the effects caused by soil and background on the canopy temperature.

Modeling the effects of LAI and chlorophyll levels on the NDVI and the R_{550}/R_{670} index

Opium poppy plants infected by *P. arborescens* at initial stages of development (until rosette stage and before stalk formation) showed a reduction in growth, which resulted in lower LAI levels and chlorophyll content degradation (assessed by visual inspection). The potential effects of such leaf density and chlorophyll decrease on the multi-spectral indices used in this study were assessed using radiative transfer modeling methods. The aim of the simulations was to obtain further insight on the changes observed in the airborne-derived multi-spectral indices due to disease stress and to verify whether they were consistent with the simulations. Moreover, the relationship between the NDVI and the R_{550}/R_{670} ratio used later for the quantitative assessment of the airborne imagery required a closer evaluation to understand the effects of chlorophyll in the red region and the decrease in the infrared region due to reduced scattering (lower LAI) in affected pixels.

Simulations were conducted with the PROSPECT leaf model (Jacquemoud and Baret 1990) coupled with the canopy-level SAILH model (Verhoef 1984) to simulate the canopy reflectance of the opium poppy field as a function of varying leaf pigment content and canopy LAI. The coupled PROSPECT + SAILH model has been used to assess the effects of plant growth variability (LAI) and leaf C_{a+b} content levels on the NDVI and the R_{550}/R_{670} ratio used in this study to detect the effects of DM. The inputs used to run the PROSPECT + SAILH model in this study are shown in Table 1.

Synthetic spectra were generated with the PROSPECT + SAILH model using as input parameters the chlorophyll content C_{ab} (20–80 μg/cm^2 in 20 μg/cm^2 steps) and the leaf area index LAI (1–5 in 1 steps) (Fig. 5). The NDVI and R_{550}/R_{670} indices were calculated for each simulated spectrum using 670 nm and 800 nm bands for the NDVI and 550 nm and 670 nm bands for the R_{550}/R_{670} index. Canopy reflectance simulations enabled the assessment of the chlorophyll content and leaf area index changes in these vegetation indices. For clusters of similar NDVI values, the variation of the R_{550}/R_{670} index and canopy temperature as a function of disease incidence was assessed in each field on each flight date.

Data analyses

The airborne data and indices calculated were subjected to a standard analysis of variance (ANOVA) using the general linear model (GLM) SAS 9.2 procedure (SAS Institute Inc.,

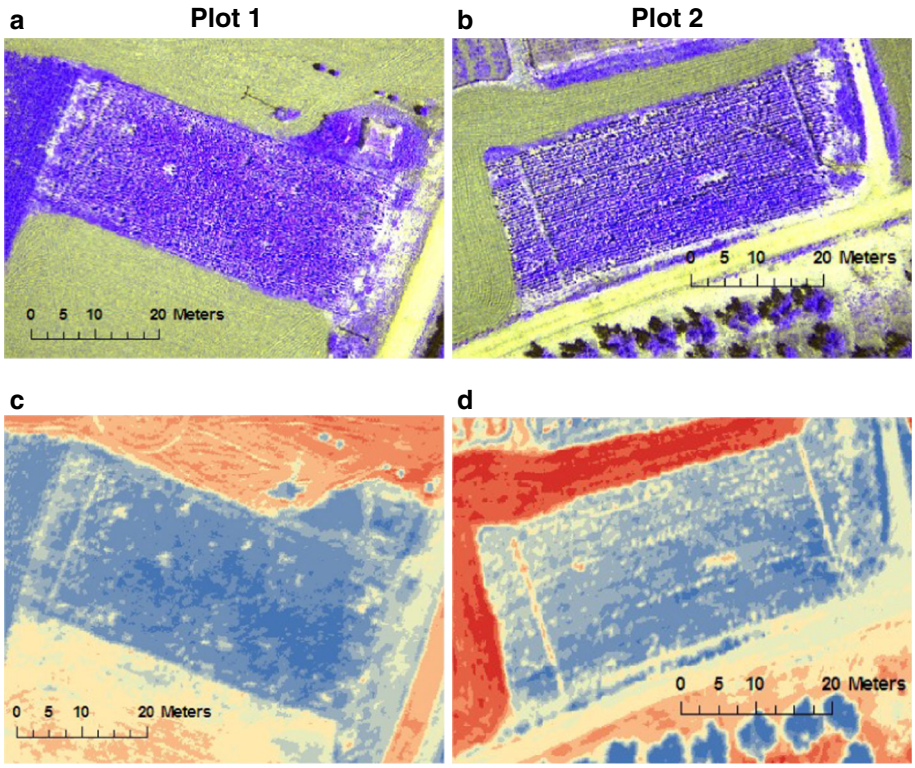

Fig. 2 Multi-spectral (**a**, **b**) and thermal (**c**, **d**) scenes obtained on 4 May 2009 with the multi-spectral and thermal cameras, respectively, on board the UAV platform at 200-mm resolution, showing Plots 1 (**a**, **c**) and 2 (**b**, **d**)

NC, USA). The ANOVA test was used to determine significant differences between asymptomatic and symptomatic plants for each NDVI step at $P < 0.05$ for (i) the canopy temperature indicators (T − Ta) and (ii) the green/red index (R_{550}/R_{670}).

Results

Downy mildew development

In Plot 1, the first symptoms of DM appeared in plants at the young rosette stage (8 to 10 leaves) by early March, reaching a global disease incidence of 0.084 %. Most diseased plants were located in the proximity of the original inoculum sources. Affected plants in Plot 1 showed typical DM symptoms indicative of systemic infection by oospores (Montes-Borrego et al. 2009b). In Plot 2, the first symptoms of DM appeared in plants at the end of the rosette stage by end of March, with a global disease incidence of 0.067 %; symptoms included small chlorotic to light-yellow leaf lesions with sporulation on the abaxial surface. By the end of April, at the end of the rosette or shooting stages in both field plots, airborne dispersion of sporangia favored

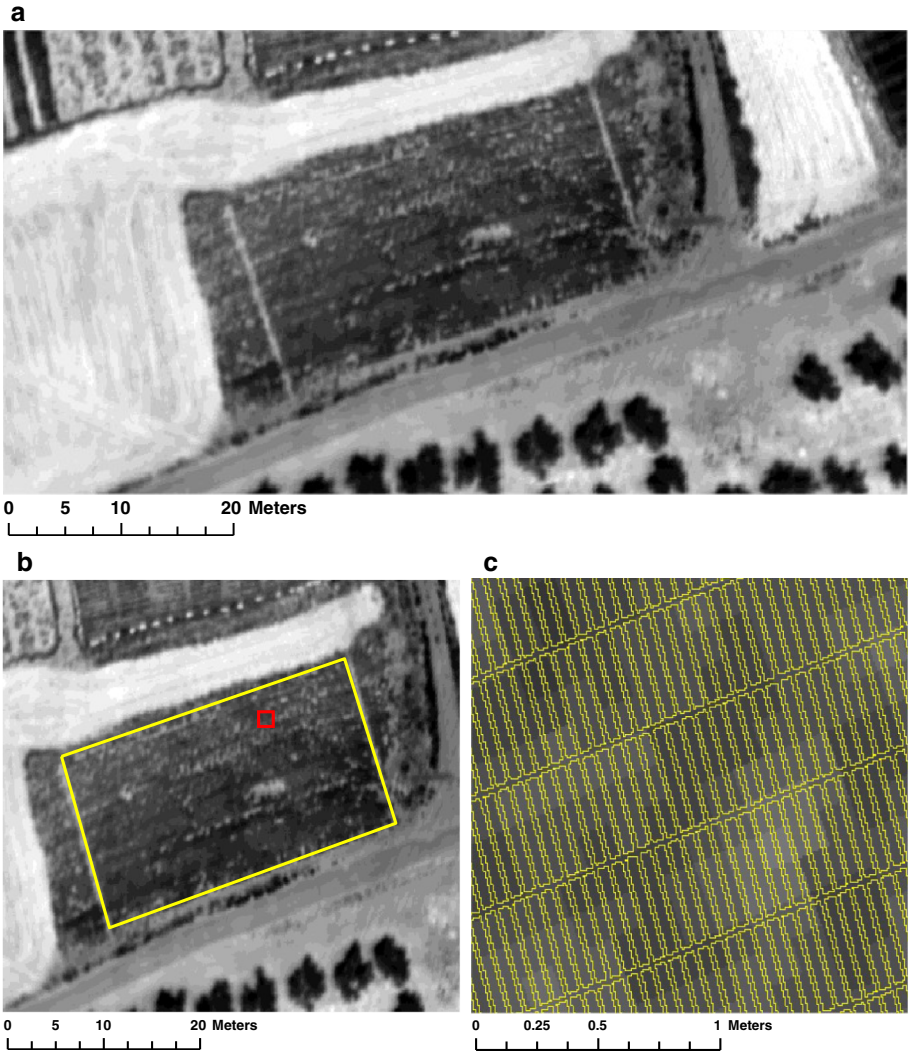

Fig. 3 Thermal scene of Plot 2 (**a**) showing the grid (**b**) that enabled single plant identification. The *red square* (**b**) shows the grid cells in detail in (**c**) (Color figure online)

the development of several small leaf lesions with intense sporulation on the abaxial surface. At this time, disease incidence had increased up to 12.0 % in both field plots and symptomatic plants were in distinct foci of disease patches throughout the fields. Later on, in early May, at the mid-flowering and capsule formation stages, disease symptoms included small chlorotic to light-yellow leaf lesions with sporulation and generalized chlorosis, curling and deformation of the young leaf blade with abundant sporulation and deformations and curling of the main flower peduncle and capsule stalk. Disease incidence reached 13.3 and 12.6 % in plots 1 and 2, respectively.

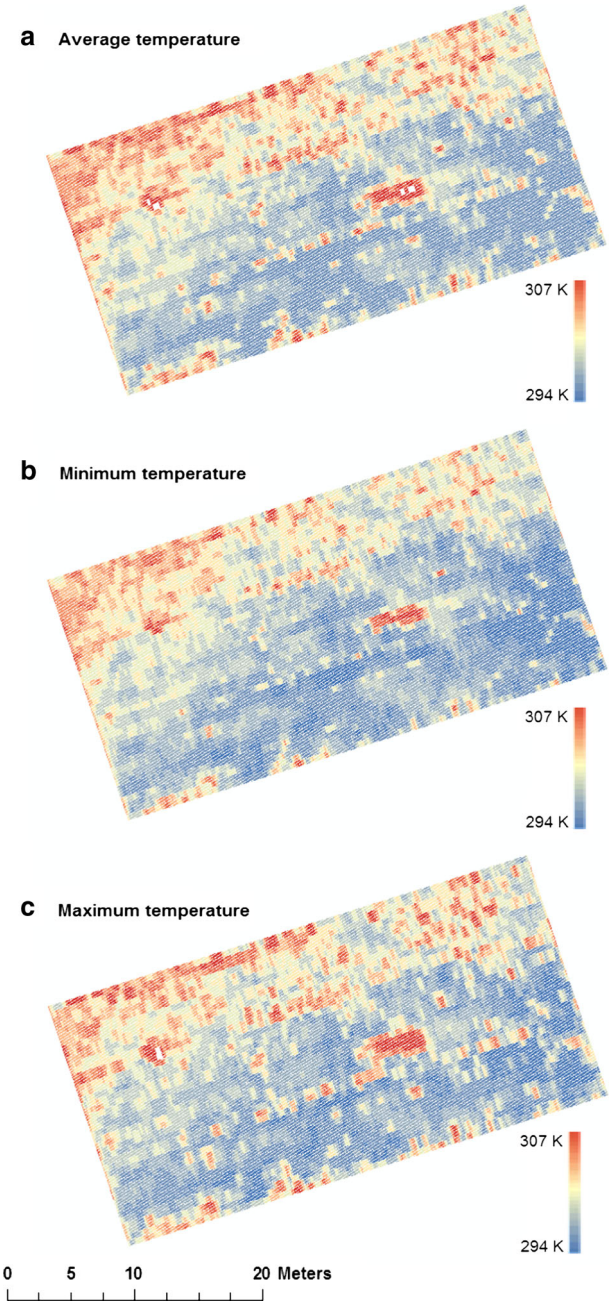

Fig. 4 Maps of Plot 2 on 4 May showing average (**a**), minimum (**b**) and maximum temperature (**c**)

Leaf measurement results

Reflectance spectra obtained by the integrating sphere for DM asymptomatic and symptomatic leaves are shown in Fig. 1a, b. Reflectance of symptomatic leaves in the visible

Table 1 PROSPECT + SAILH model inputs used in this study to assess the effects of downy mildew on spectral indices in opium poppy

PROSPECT-SAILH inputs	Values
Leaf optical and structural parameters	
Leaf structural parameter (N)	1.25
Chlorophyll content (C_{ab})	20–80 μg/cm^2
Water equivalent thickness (C_w)	0.025 cm
Dry matter content (C_m)	0.01 g/cm^2
Brown pigment content (C_s)	0
Canopy layer and structural parameters	
Leaf area index (LAI)	1–5
Leaf angle distribution (LAD)	Plagiophile
Hot spot size (h)	0.1
Background and viewing geometry	
Solar zenith angle (Sza)	30°
Viewing zenith angle (Vza)	0°
Relative azimuth angle (Raz)	0°
Soil reflectance (ρ_s)	From image

Parameters C_{ab} and LAI varied randomly within the range indicated on the table

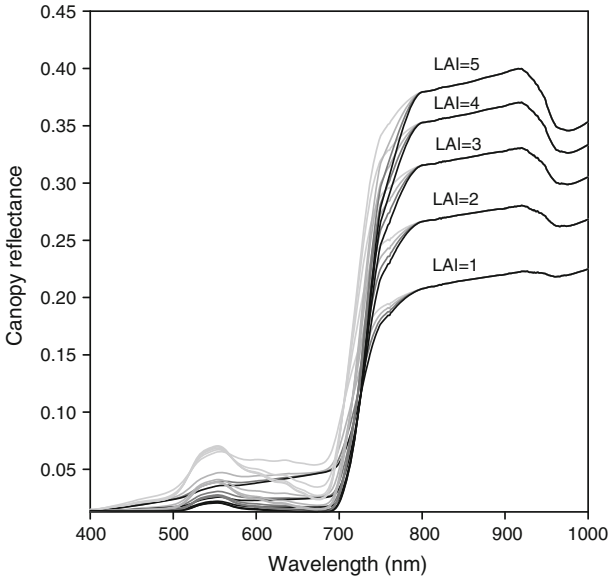

Fig. 5 Simulated canopy reflectance at 1 nm resolution using the PROSPECT + SAILH model. The effects of LAI and chlorophyll content C_{ab} on canopy reflectance are shown

(VIS) green range (550 nm) and red-edge region (650–720 nm) was higher than that of asymptomatic leaves due to the decrease in C_{ab} content caused by DM infection. Therefore, these differences in reflectance spectra between asymptomatic and symptomatic leaves were detected using the NDVI and R_{550}/R_{670} indices calculated from the imagery. DM asymptomatic leaves showed significantly higher or lower ($P < 0.05$) NDVI and

R_{550}/R_{670} values than DM symptomatic leaves (Fig. 6). These results agree with those of the simulation study described above.

Modeling results

The modeling results for the NDVI and R_{550}/R_{670} indices calculated for each simulated spectrum as a function of LAI and leaf C_{ab} variation are shown in Fig. 7. The NDVI was positively related to LAI and C_{ab} content (Fig. 7a). Changes in LAI between 1 and 5 were captured by the NDVI; yet, the differences in C_{ab} content had small effects on the NDVI, reaching a saturation on the NDVI for $C_{ab} > 40$ μg/cm^2. In addition, the effects on the NDVI due to C_{ab} degradation were extremely low even for $C_{ab} < 40$ μg/cm^2. However, the second index proposed in this study—R_{550}/R_{670}—was inversely related to C_{ab} content and showed high sensitivity to C_{ab} content changes (Fig. 7b). The sensitivity of the R_{550}/R_{670} ratio to C_{ab} content increased with higher LAI values, showing large effects on this index for lower C_{ab} content levels. The simulations demonstrated that the proposed R_{550}/R_{670} ratio is sensitive to chlorophyll content but is also affected by LAI, while the NDVI is a primary indicator of LAI only.

The R_{550}/R_{670} vs. NDVI chart (Fig. 8) for various pigment content and LAI levels shows that, for a given NDVI value, chlorotic pixels deviated towards the upper part of the chart. Thus, the NDVI vs. R_{550}/R_{670} relationship obtained as a function of LAI and C_{ab} ranges illustrates the potentially expected deviation of the relationship from healthy (high chlorophyll content and high LAI values) to diseased plants (i.e. chlorotic plants with lower C_{ab} and lower growth yielding lower LAI values). The R_{550}/R_{670} index was related to the NDVI, yielding the same value (for example $R_{550}/R_{670} = 1.5$) for both low (NDVI = 0.7, LAI = 2, $C_{ab} = 20$) and high NDVI values (NDVI = 0.93, LAI = 5, $C_{ab} = 80$). Simulations demonstrated that, for a specific NDVI value, higher R_{550}/R_{670} values could be expected for plants with lower chlorophyll content. Due to the relationship obtained between the R_{550}/R_{670} index and the NDVI, the assessment of DM infection using the R_{550}/R_{670} ratio was conducted at the image level as a function of the NDVI in clusters with values between 0.4 and 1.0. Therefore, after this simulation study was conducted, the

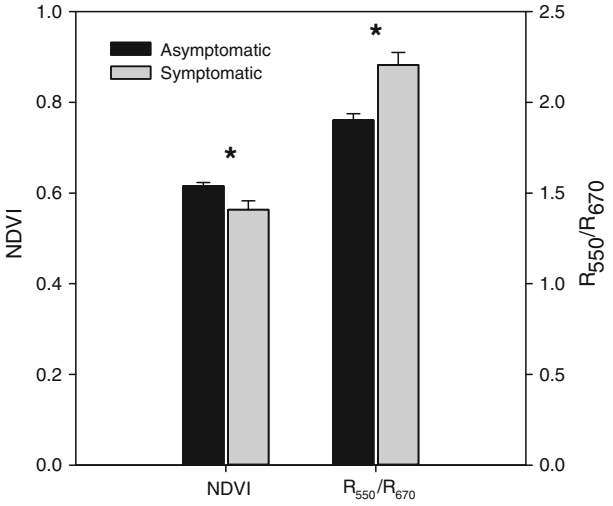

Fig. 6 Mean measurements of NDVI and R_{550}/R_{670} measurements for DM asymptomatic and symptomatic leaves. *Asterisks* indicate significant differences between DM symptomatic and asymptomatic leaves according to an ANOVA at $P < 0.05$. *Error bars* indicate standard errors

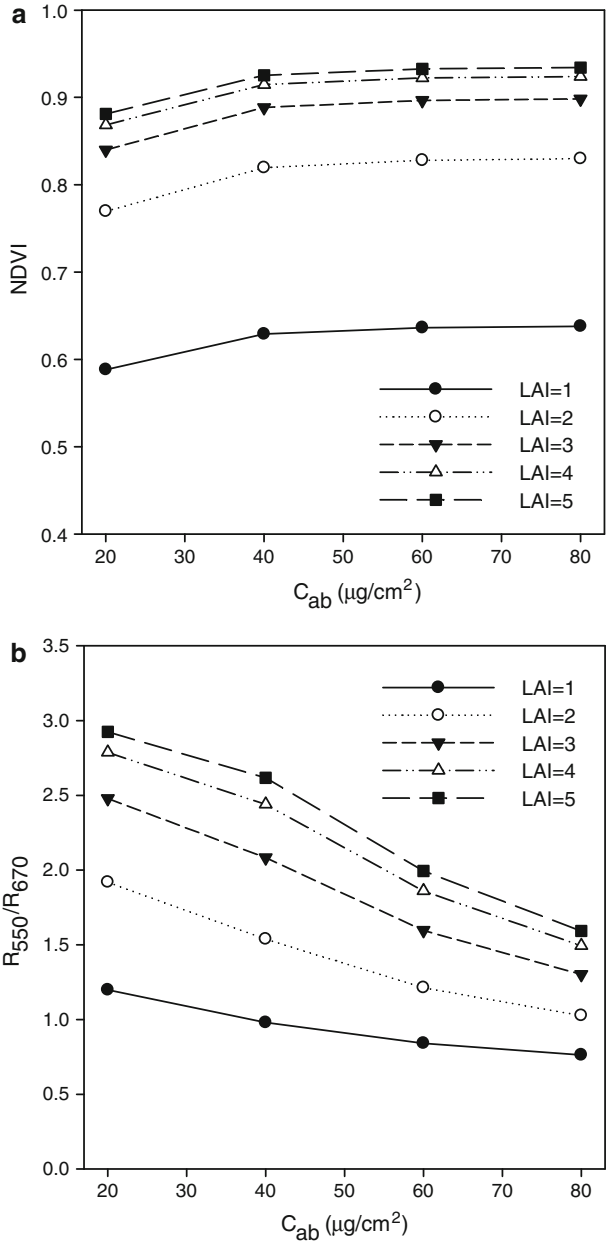

Fig. 7 Modeling simulations performed with the PROSPECT + SAILH model to assess the effects of LAI and C_{ab} on the NDVI (**a**) and R_{550}/R_{670} (**b**) indices used in this study

hypothesis under study was that, for each NDVI cluster, the image blocks showing higher R_{550}/R_{670} values would probably be more affected by DM. The statistical analysis assessed the distinction between diseased and healthy image blocks as a function of NDVI step. These results are consistent with those obtained at leaf level.

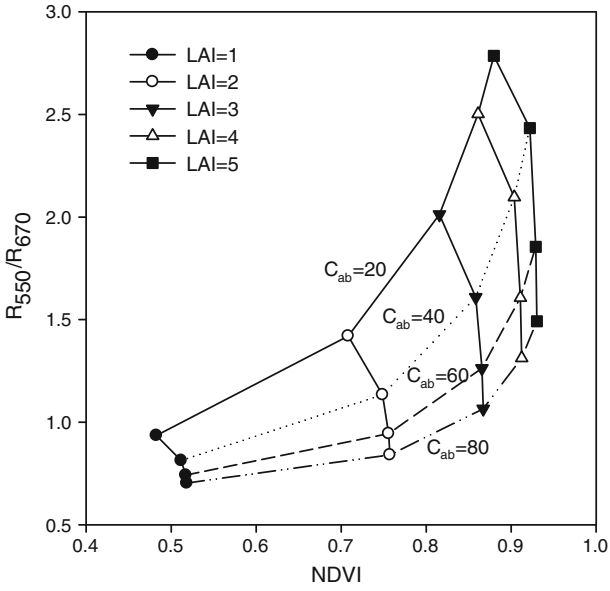

Fig. 8 Relationship between the R_{550}/R_{670} and the NDVI at different LAI and C_{ab} content levels

Results of the statistical analysis conducted on the thermal and multi-spectral airborne imagery

The grid created from the high-resolution multi-spectral and thermal imagery enabled the assessment of each single image block by comparing it against DM incidence recorded in the field. The maps generated represent the spatial pattern of canopy temperature normalized by air temperature (Tc − Ta), the NDVI and the R_{550}/R_{670} index as indicators of DM incidence for each opium poppy plot (Figs. 9, 10). Such maps showed a negative correlation between Tc − Ta and the NDVI and between Tc − Ta and the R_{550}/R_{670} index. Thus, areas with low NDVI values showed high temperatures due to the low LAI and large soil effects on the image blocks with low canopy densities.

Table 2 shows the statistical assessment of T_{avg}, T_{max}, T_{min} normalized by Ta and of the R_{550}/R_{670} ratio calculated from each image block for healthy and DM symptomatic plants on both dates and fields according to an ANOVA ($P < 0.05$) as a function of NDVI step. The ANOVA shows that T_{avg} and T_{max} were not able to distinguish between the two classes; T_{min} was the only temperature value that was sensitive to both DM symptomatic and healthy plants. Thus, T_{min} of asymptomatic plants was lower and showed greater variability compared to that of DM symptomatic plants. Results for T_{min} − Ta are shown in Fig. 11, which shows that T_{min} − Ta tended to decrease as NDVI increased in DM symptomatic plants, showing a significantly higher ($P < 0.05$) temperature than asymptomatic plants at NDVI steps > 0.6. In Field plot 1, the temperature was significantly higher ($P < 0.05$) in symptomatic plants than in asymptomatic plants for $0.6 \leq \text{NDVI} < 0.9$ on 24 April and 4 May (Fig. 11a, b). In Field plot 2, higher temperature values for symptomatic plants at significant levels ($P < 0.05$) were recorded for $0.6 \leq \text{NDVI} < 0.9$ and $0.6 \leq \text{NDVI} \leq 1.0$ on 24 April and 4 May, respectively (Fig. 11c,d). At low NDVI values (NDVI < 0.6), canopy temperature in symptomatic and asymptomatic plants did not differ significantly ($P \geq 0.05$), probably due to structural changes, plant senescence and death in plants severely damaged by the pathogen.

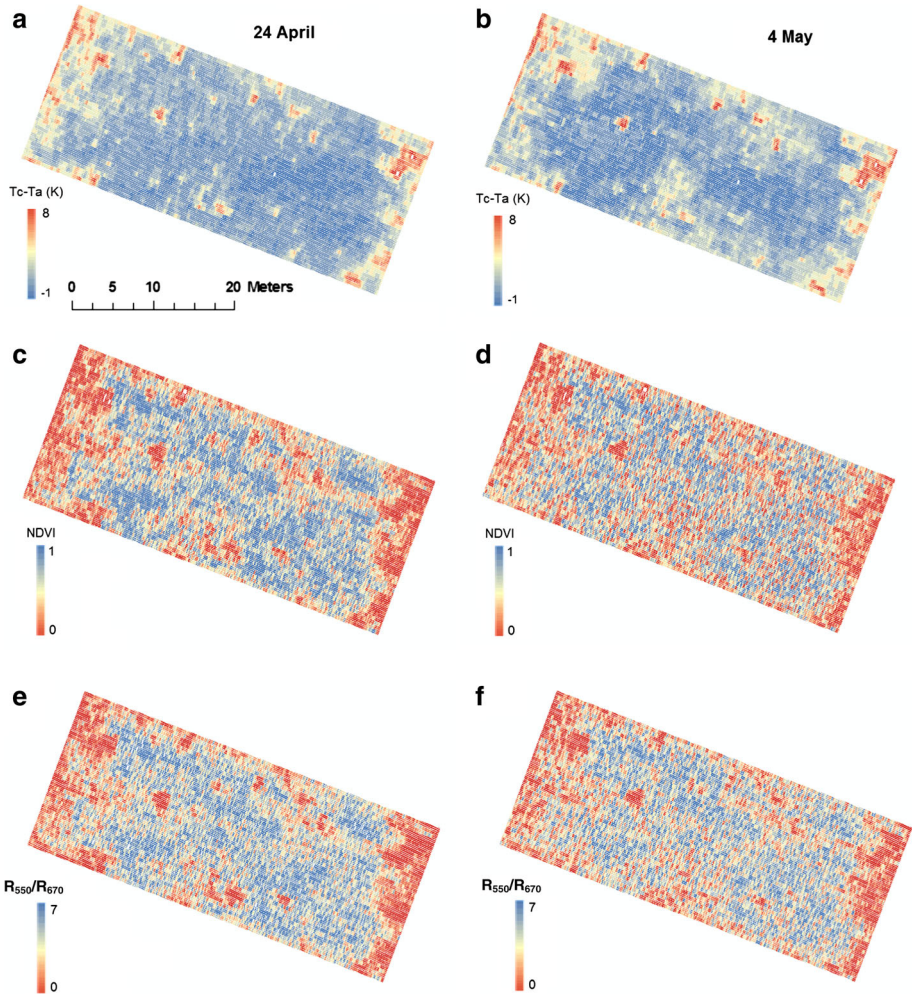

Fig. 9 Spatial distribution of canopy Tc − Ta (**a**, **b**), NDVI (**c**, **d**) and R_{550}/R_{670} (**e**, **f**) for Plot 1 on 24 April (**a**, **c**, **e**) and 4 May (**b**, **d**, **f**)

Results obtained for the R_{550}/R_{670} index as a function of the same NDVI steps (Table 2; Fig. 12) showed an upward trend as NDVI increased. R_{550}/R_{670} was able to detect DM, showing significantly higher values ($P < 0.05$) for symptomatic plants at an NDVI ≥ 0.5. In Field plot 1, these differences were recorded for $0.5 \leq$ NDVI ≤ 0.9 in images taken on 24 April and 4 May (Fig. 12a, b); in Field plot 2, significant differences were found for $0.3 \leq$ NDVI ≤ 0.9 and $0.4 \leq$ NDVI ≤ 1.0 on 24 April and 4 May, respectively (Fig. 12c, d). Thus, the R_{550}/R_{670} index detected a decrease in chlorophyll content at high NDVI steps for DM symptomatic plants. As happened with temperature, no significant differences ($P \geq 0.05$) were found between DM symptomatic and asymptomatic plants in the R_{550}/R_{670} index at low NDVI values. This was probably due to structural changes related to plant death in blocks that were severely affected by the pathogen and had large background/soil effects on the calculated index. Nevertheless, the combination of the NDVI

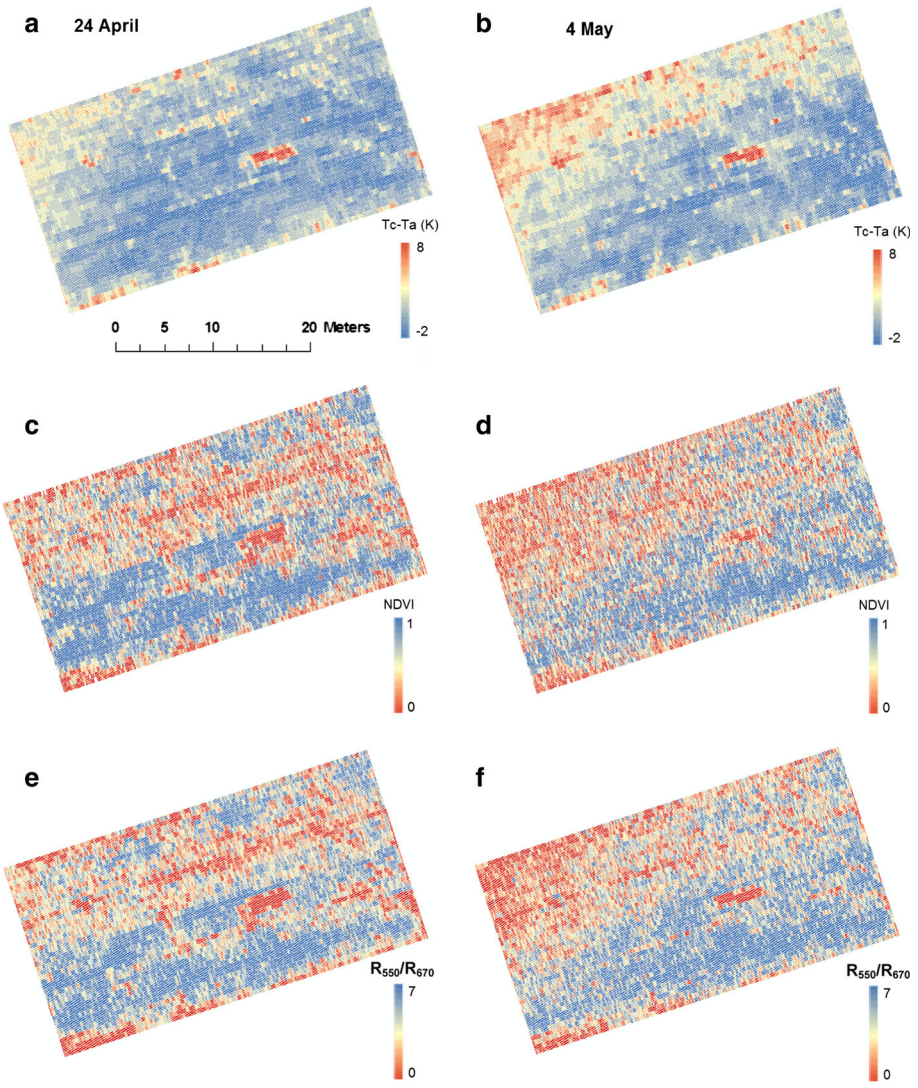

Fig. 10 Spatial distribution of canopy Tc − Ta (**a**, **b**), NDVI (**c**, **d**) and R_{550}/R_{670} (**e**, **f**) for Plot 2 on 24 April (**a**, **c**, **e**) and 4 May (**b**, **d**, **f**)

with the R_{550}/R_{670} index was more effective in distinguishing between DM symptomatic and asymptomatic plants at lower NDVI steps than when using thermal indicators. In Field plot 2, for instance, DM symptomatic and asymptomatic plants were differentiated along the entire NDVI range for virtually all classes, while the thermal data failed at low LAI levels.

The relationship between the R_{550}/R_{670} ratio and the NDVI shown in Fig. 12 was consistent with the simulation analysis conducted with the coupled PROSPECT + SAILH model shown in Fig. 8. In both figures, for a given NDVI step, a decrease in C_{ab} content (symptomatic plants) was accompanied by an increase in the R_{550}/R_{670} index.

Table 2 Results of statistical analyses for T_{avg}, T_{max}, T_{min} normalized by Ta, and for the R_{550}/R_{670} ratio calculated from each image block on both dates and in both fields as a function of NDVI step

NDVI range	T_{min} − Ta				T_{avg} − Ta				T_{max} − Ta				R_{550}/R_{670}			
	Plot 1		Plot 2		Plot 1		Plot 2		Plot 1		Plot 2		Plot 1		Plot 2	
	04/24	05/04	04/24	05/04	04/24	05/04	04/24	05/04	04/24	05/04	04/24	05/04	04/24	05/04	04/24	05/04
0.3–0.4															*	
0.4–0.5															*	*
0.5–0.6													*	*	*	*
0.6–0.7	*	*	*	*	*	*				*			*	*	*	*
0.7–0.8	*	*	*	*									*	*	*	*
0.8–0.9	*	*	*	*		*							*	*	*	*
0.9–1.0				*				*								*

Asterisks indicate significant differences between DM asymptomatic and symptomatic plants according to an ANOVA test at $P < 0.05$

Discussion

DM infected plants show a physiological reaction to infection by the pathogen that results in a change of spectral reflectance due to the decreasing chlorophyll content and changing internal structure. Chlorophyll content tends to decrease in DM infected plants, showing a higher reflectance in the visible green region that is correlated with the severity of symptoms. Plants under disease stress also show internal structural changes that lead to a decrease of spectral reflectance in the near-infrared (NIR) range. In addition, DM pathogens penetrate stomata and cause excessive transpiration that rapidly leads to a decrease in water content. This malfunction of stomata eventually results in the desiccation of leaf tissue and an increase in temperature (Lindenthal et al. 2005; Oerke et al. 2006). Considering these changes, the hypothesis was that DM disease symptoms could be detected remotely in the following regions: the visible (400–700 nm) and red-edge (670–750 nm) spectral region, due to the necrotic and chlorotic lesions caused by chlorophyll degradation; the NIR region (800 nm) due to changes in canopy density and leaf area; and the thermal-infrared region because of the changes in the transpiration rate that affect canopy temperature. Despite the various potential remote sensing indices that can be used for disease detection, very few studies have been conducted with combined indices from different spectral domains (i.e. structural, chlorophyll and thermal spectral regions). Consequently, three indices including these spectral regions were explored in this study: the R_{550}/R_{670} for the detection of chlorophyll content, the NDVI to detect structural changes and the Tc − Ta as an indicator of canopy transpiration levels.

Remote sensing has been extensively applied to detecting foliar diseases in annual agricultural crops, mostly using the NDVI, which is closely related to green biomass (Bravo et al. 2003; Steddom et al. 2005; Franke and Menz 2007; Mahlein et al. 2010; Rumpf et al. 2010). In DM infected canopies, visible reflectance increases and NIR reflectance decreases, resulting in lower green canopy biomass and consequently lower NDVI values. However, few studies have examined the relationship between chlorophyll content and spectral reflectance obtained from a diseased canopy. Although chlorosis and necrosis have long been assumed to be associated with DM infection, no studies have been

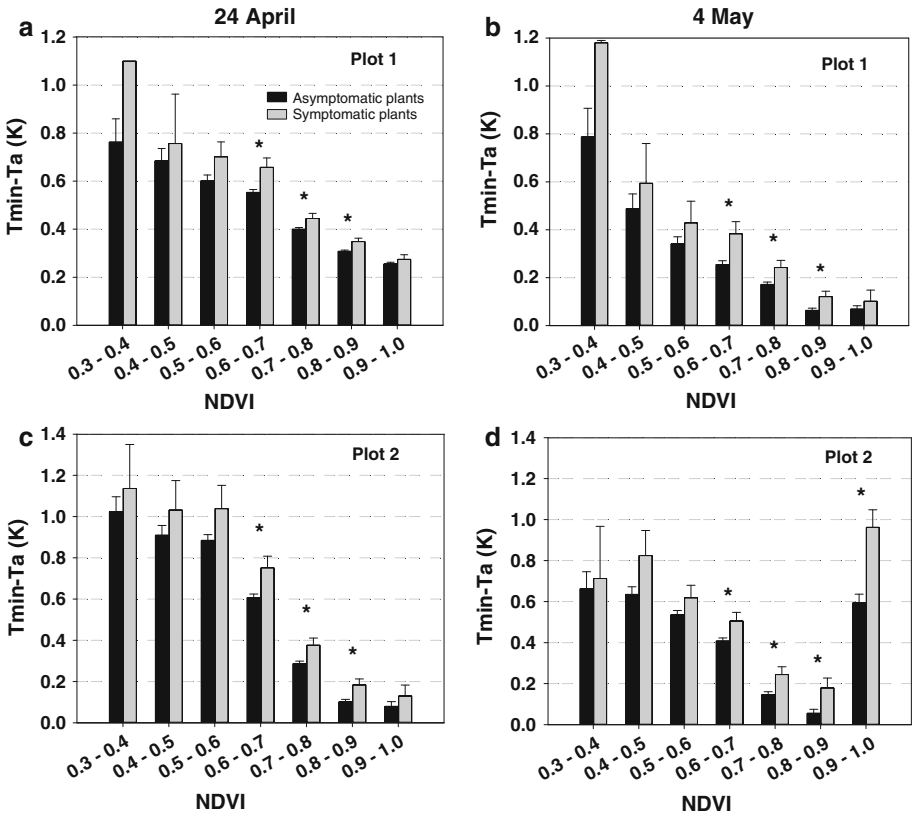

Fig. 11 Relationship between minimum temperature Tc − Ta and the NDVI on 24 April 2009 (**a**, **c**) and 4 May 2009 (**b**, **d**) for DM asymptomatic and symptomatic plants in Field Plot 1 (**a**, **b**) and plot 2 (**c**, **d**). Asterisks indicate significant differences between symptomatic and asymptomatic plants according to an ANOVA at $P < 0.05$. On 24 April, 15 153 and 18 026 healthy plants and 1 811 and 2 290 DM symptomatic plants were analyzed for plot 1 and 2, respectively. On 5 May, 13 713 and 11 411 healthy plants and 1 936 and 1 665 symptomatic plants were analyzed for plot 1 and 2, respectively. *Error bars* indicate standard errors

conducted to directly explore the impact of DM on chlorophyll content in plants growing under field conditions. Distinct color changes are evident on the aboveground parts of DM infected plants (green leaves become chlorotic, yellow and brown), demonstrating the potential of remote sensing for DM detection.

Thermal imagery has successfully been used to identify water stress at early stages (Berni et al. 2009a, b; Zarco-Tejada et al. 2012). Moreover, foliar temperature of DM infected cucumber plants has been proven to rise when chlorotic and necrotic tissues appear (Lindenthal et al. 2005; Oerke et al. 2006). Therefore, the importance of thermal imagery as an adequate indicator of low transpiration rates induced by water or disease stress is evident. However, thermal imaging is restricted to medium-resolution sensors in current satellites due to technical limitations (Berni et al. 2009a) and provides spatial resolutions of 90 and 100 m pixel size. This limited resolution of thermal imagery acquired from satellites is a clear drawback when very high resolution (VHR) imagery is needed. Manned and unmanned airborne platforms are the alternative for vegetation monitoring

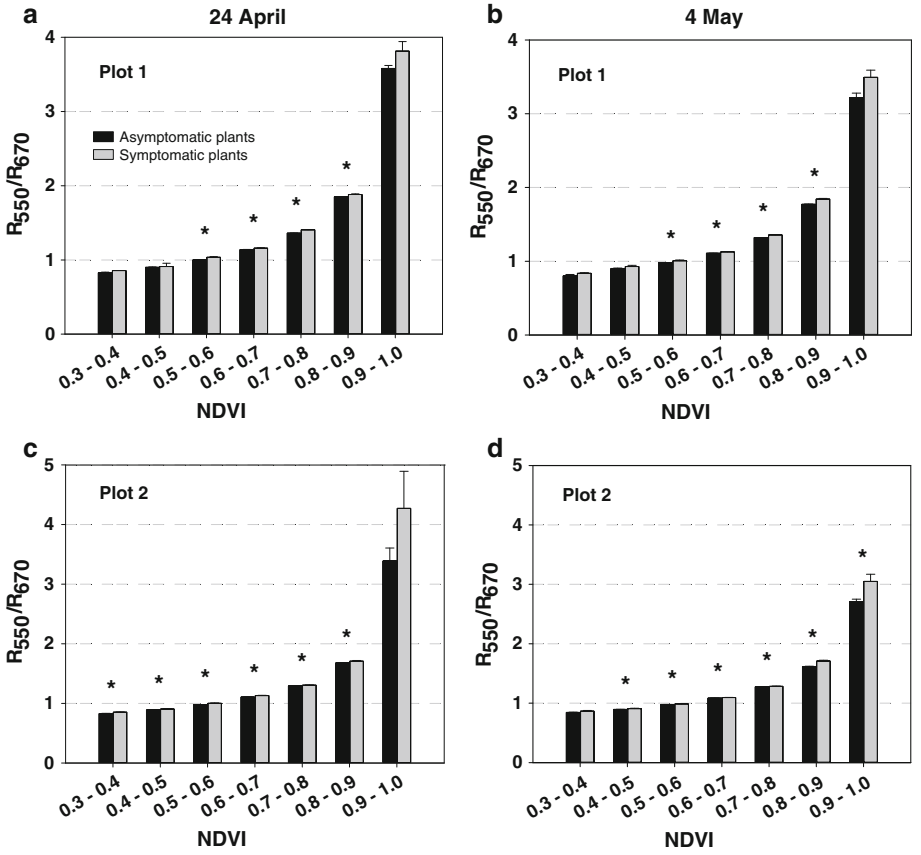

Fig. 12 Relationship between the R_{550}/R_{670} and the NDVI on 24 April 2009 (**a**, **c**) and 4 May 2009 (**b**, **d**) for DM asymptomatic and symptomatic plants in Plot 1 (**a**, **b**) and Plot 2 (**c**, **d**). *Asterisks* indicate significant differences between symptomatic and asymptomatic plants according to an ANOVA at $P < 0.05$. On 24 April, 15 153 and 18 026 healthy plants and 1 811 and 2 290 DM symptomatic plants were analyzed for plot 1 and 2, respectively. On 5 May, 13 713 and 11 411 healthy plants and 1 936 and 1 665 symptomatic plants were analyzed for plot 1 and 2, respectively. *Error bars* indicate standard errors

using thermal imagery due to the sub-meter spatial resolution they provide. Similarly, the low spatial resolution acquired in the visible and NIR regions is acceptable for classifying crops in large farms (Zaitseva et al. 1997; Srinivas et al. 2004). Yet, VHR imagery is required for stress detection within individual crop fields (Berni et al. 2009a, b; Suárez et al. 2010; Zarco-Tejada et al. 2012). In this study, VHR airborne imagery was acquired to obtain pure vegetation pixels and to minimize background, shadow and soil effects on the pixels used to detect small differences between asymptomatic and symptomatic plants in thermal and multi-spectral indices. Indeed, VHR acquired from airborne platforms is the alternative to medium-resolution imagery, which aggregates pixels and makes it difficult to assess intra-plot variability and detect focal points of the disease.

Simulations conducted with PROSPECT + SAILH for varying chlorophyll content and canopy LAI were consistent with the image-retrieved indices used to assess DM infection. Infected plants showed leaf chlorosis and necrosis, which resulted in chlorophyll content

degradation and canopy density and leaf area reduction as well as higher R_{550}/R_{670} and lower NDVI values. Simulation results confirmed those obtained from leaf-level measurements and multi-spectral imagery. Leaf measurements conducted with the integrating sphere were able to distinguish between DM asymptomatic and symptomatic leaves due to the significant spectral differences registered in the visible, red edge and near infrared regions. Airborne flights conducted with thermal and multi-spectral cameras enabled accurate DM detection at high NDVI steps by using the Tc − Ta and R_{550}/R_{670} indicators. At low NDVI steps, differences in Tc − Ta and R_{550}/R_{670} between asymptomatic and symptomatic plants were not detected, probably due to the effect of structural and background effects on the pixels (a decrease in green biomass caused by senescence and death in plants severely damaged by DM). To the extent of the authors' knowledge, no studies have been conducted to identify DM infection using chlorophyll content indices. However, studies with foliar temperature have been conducted by (Lindenthal et al. 2005) and Oerke et al. (2006) in cucumber plants affected by DM at leaf level, showing a decrease in the transpiration rate and a consequent rise in temperature with the appearance of chlorotic and necrotic tissues. The results presented were obtained from imagery acquired with a low-cost multi-spectral camera and a miniaturized thermal camera on board a 2-m wingspan UAV. This demonstrates the potential relevance and implications for disease detection at field level based on reliable remote sensing methods. Further studies should focus on the use of hyperspectral sensors that provide a larger number of physiological indices. Narrow-band indices calculated from hyperspectral data have been proven to have more variability for detecting physiological changes than wide-band multi-spectral indices (Yang et al. 2009).

Conclusions

In the present study, the ability of remote sensing methods to detect DM symptoms in two opium poppy plots with two different initial sources of inoculum was assessed. Techniques were applied based on the detection of the effects of *P. arborescens* infection and leaf colonization on transpiration rate using the thermal and multi-spectral domains. High-resolution imagery was acquired with a thermal and a multi-spectral camera installed on board a UAV to extract mean thermal and spectral reflectance for each plant by using a grid with the same dimensions as each plot. This grid made possible the assessment of each single block by comparing the incidence of DM recorded in the field. Results demonstrated that canopy temperature (Tc − Ta) and the green/red ratio (R_{550}/R_{670}) were related to physiological stress caused by DM infection at high NDVI steps. At low NDVI values, Tc − Ta and the R_{550}/R_{670} index were not significantly different ($P \geq 0.05$) between symptomatic and asymptomatic plants; this was probably due to structural changes, plant senescence and death in plants severely damaged by the pathogen. Leaf measurements showed higher reflectance in the visible, red-edge and near infrared spectral ranges for symptomatic leaves due to their lower chlorophyll content and greater structural damage. This enabled the identification of infected plants by using the NDVI and R_{550}/R_{670} indices, which recorded significant differences ($P < 0.05$) between asymptomatic and symptomatic leaves. Modeling simulations were conducted with the coupled PROSPECT + SAILH model to simulate the effects of varying chlorophyll content and canopy LAI on the NDVI and R_{550}/R_{670} indices extracted from the multi-spectral imagery, confirming the results obtained from the leaf measurements and the multi-spectral airborne flights using an UAV. This study represents progress in the development of methods to detect *P. arborescens*

infection in opium poppy plants using high-resolution thermal and multi-spectral imagery acquired with low-cost cameras on board UAVs for remote sensing purposes.

Acknowledgments Financial support for this research was provided by the Spanish Ministry of Education and Science through projects AGL2009-13105, AGL2012-40053-C03-01 and PET2006_0444, the Regional Government of Andalusia through project P10-AGR-6497 and the European Union through the European Regional Development Fund (ERDF). R. Calderón was supported by research fellowship BES-2010-035511 from the Spanish Ministry of Education and Science. D. Notario, A. Vera, A. Hornero, R. Romero and A. Gómez are acknowledged for their support during the airborne campaigns and the image processing. We are also grateful to C. Cantalapiedra, F. Durán, G. León-Ropero, M. Medina and J.L. Trapero-Casas for their excellent technical support.

References

Barton, C. (2012). Advances in remote sensing of plant stress. *Plant and Soil, 354*, 41–44.

Berni, J. A. J., Zarco-Tejada, P. J., Sepulcre-Cantó, G., Fereres, E., & Villalobos, F. J. (2009a). Mapping canopy conductance and CWSI in olive orchards using high resolution thermal remote sensing imagery. *Remote Sensing of Environment, 113*, 2380–2388.

Berni, J. A. J., Zarco-Tejada, P. J., Suárez, L., & Fereres, E. (2009b). Thermal and narrow-band multispectral remote sensing for vegetation monitoring from an unmanned aerial vehicle. *IEEE Transactions on Geoscience and Remote Sensing, 47*, 722–738.

Bravo, C., Moshou, D., West, J., McCartnet, A., & Ramon, H. (2003). Early disease Detection in Wheat Fields using spectral Reflectance. *Biosystems Engineering, 84*(2), 137–145.

Franke, J., & Menz, G. (2007). Multi-temporal wheat disease detection by multi-spectral remote sensing. *Precision Agriculture, 8*, 161–172.

Gueymard, C. A. (1995). SMARTS, a simple model of the atmospheric radiative transfer of sunshine: Algorithms and performance assessment. Technical report no. FSEC-PF-270-95. Cocoa, FL: Florida Solar Energy Center.

Gueymard, C. A. (2001). Parameterized transmittance model for direct beam and circumsolar spectral irradiance. *Solar Energy, 71*, 325–346.

Herwitz, S., Johnson, L., Dunagan, S., Higgins, R., Sullivan, D., Zheng, J., et al. (2004). Imaging from an unmanned aerial vehicle: Agricultural surveillance and decision support. *Computers and Electronics in Agriculture, 44*, 49–61.

Ingram, D. S. (1981). Physiology and biochemistry of host-parasite interaction. In D. M. Spencer (Ed.), *The downy mildews* (pp. 143–163). London: Academic Press.

Jacquemoud, S., & Baret, F. (1990). PROSPECT: A model of leaf optical properties spectra. *Remote Sensing of Environment, 34*, 75–91.

Kapoor, L. D. (1995). *Opium Poppy: Botany, Chemistry, and Pharmacology*. Binghampton, NY: Haworth Press.

Khristov, A. (1943). Fungi causing spot on the balls and moulding the seed of opium poppy. *Bulgaria Agricultural Experiment Station Journal, 13*, 13–19.

Landa, B. B., Montes-Borrego, M., Muñoz-Ledesma, F. J., & Jiménez-Díaz, R. M. (2005). First report of downy mildew of opium poppy caused by *Peronospora arborescens* in Spain. *Plant Disease, 89*, 338.

Landa, B. B., Montes-Borrego, M., Muñoz-Ledesma, F. J., & Jiménez-Díaz, R. M. (2007). Phylogenetic analysis of downy mildew pathogens of opium poppy and PCR-based in planta and seed detection of *Peronospora arborescens*. *Phytopathology, 97*, 1380–1390.

Lindenthal, M., Steiner, U., Dehne, H.-W., & Oerke, E.-C. (2005). Effect of downy mildew development on transpiration of cucumber leaves visualized by digital infrared thermography. *Phytopathology, 95*(3), 233–240.

Mahlein, A.-K., Steiner, U., Dehne, H.-W., & Oerke, E.-C. (2010). Spectral signatures of sugar beet leaves for the detection and differentiation of diseases. *Precision Agriculture, 11*, 413–431.

Montes-Borrego, M., Muñoz-Ledesma, F. J., Jiménez-Díaz, R. M., & Landa, B. B. (2009a). A nested-PCR protocol for detection and population biology studies of *Peronospora arborescens*, the downy mildew pathogen of opium poppy, using herbarium specimens and asymptomatic, fresh plant tissues. *Phytopathology, 99*, 73–81.

Montes-Borrego, M., Muñoz-Ledesma, F. J., Jiménez-Díaz, R. M., & Landa, B. B. (2011). Real-Time PCR quantification of *Peronospora arborescens*, the opium poppy downy mildew pathogen, in seed stocks and symptomless infected plants. *Plant Disease, 95*, 143–152.

Montes-Borrego, M., Navas-Cortés, J. A., Muñoz-Ledesma, F. J., Jiménez-Díaz, R. M., & Landa, B. B. (2009b). Role of oospores as primary inoculum for epidemics of downy mildew caused by *Peronospora arborescens* in opium poppy crops in Spain. *Plant Pathology, 58*, 1092–1103.

Navas-Cortés, J. A., Montes-Borrego, M., Muñoz-Ledesma, F. J., Jiménez-Díaz, R. M., & Landa, B. B. (2009). Soil-borne oospores of *Peronospora arborescens* as a major primary inoculum for opium poppy downy mildew epidemics in Southern Spain. In D. M. Gadoury, R. C. Seem, M. M. Moyer, & W. E. Fry (Eds.), *Proceedings of the 10th International Epidemiology Workshop* (pp. 108–110). Geneva, NY: New York State Agricultural Experiment Station.

Nilsson, H. E. (1995). Remote sensing and image analysis in plant pathology. *Annual Review of Phytopathology, 15*, 489–527.

Oerke, E. C., Lindenthal, M., Fröhling, P., & Steiner, U. (2005). Digital infrared thermography for the assessment of leaf pathogens. In: Stafford J. V. (Ed.), Precision agriculture'05. *Proceedings of 5th European Conference on Precision Agriculture* (pp. 91–98). Wageningen: Wageningen Academic Publishers.

Oerke, E. C., Steiner, U., Dehne, H. W., & Lindenthal, M. (2006). Thermal imaging of cucumber leaves affected by downy mildew and environmental conditions. *Journal of Experimental Botany, 57*(9), 2121–2132.

Populer, C. (1981). Epidemiology of downy mildews. In D. M. Spencer (Ed.), *The downy mildews* (pp. 45–105). London: Academic Press.

Rouse, J. W., Haas, R. H., Schell, J. A., Deering, D. W., & Harlan, J. C. (1974). *Monitoring the vernal advancement and retrogradation (greenwave effect) of natural vegetation*. Greenbelt, MD: NASA/GSFC Type III Final Report.

Rumpf, T., Mahlein, A.-K., Steiner, U., Oerke, E.-C., Dehne, H.-W., & Plümer, L. (2010). Early detection and classification of plant diseases with support vector machines based on hyperspectral reflectance. *Computers and Electronics in Agriculture, 74*(1), 91–99.

Sankaran, S., Mishra, A., Ehsani, R., & Davis, C. (2010). A review of advanced techniques for detecting plant diseases. *Computers and Electronics in Agriculture, 72*, 1–13.

Scott, J. B., Hay, F. S., & Wilson, C. R. (2004). Phylogenetic analysis of the downy mildew pathogen of oilseed poppy in Tasmania, and its detection by PCR. *Mycological Research, 108*, 198–205.

Srinivas, P., Das, B. K., Saibaba, J., & Krishnan, R. (2004). Application of distance Based Vegetation index For Agricultural Crops Discrimination. In: O. Altan (Ed.), *Proceedings of Geo-Imagery Bridging Continents, XXth ISPRS Congress, Technical Commission VII* (pp. 1127–1132). Istanbul, Turkey: ISPRS 2004.

Steddom, K., Bredehoeft, M. W., Khan, M., & Rush, C. M. (2005). Comparison of visual and multispectral radiometric disease evaluations of cercospora leaf spot of sugar beet. *Plant Disease, 89*(2), 153–158.

Stoll, M., Schultz, H. R., Baecker, G., et al. (2008a). Early pathogen detection under different water status and the assessment of spray application in vineyards through the use of thermal imagery. *Precision Agriculture, 9*, 407–417.

Stoll, M., Schultz, H. R., & Berkelmann-Loehnertz, B. (2008b). Exploring the sensitivity of thermal imaging for *Plasmopara viticola* pathogen detection under different water status. *Functional Plant Biology, 35*, 281–288.

Suárez, L., Zarco-Tejada, P. J., González-Dugo, V., Berni, J. A. J., Sagardoy, R., Morales, F., et al. (2010). Detecting water stress effects on fruit quality in orchards with time-series PRI airborne imagery. *Remote Sensing of Environment, 114*, 286–298.

Sugiura, R., Noguchi, N., & Ishii, K. (2005). Remote-sensing technology for vegetation monitoring using an unmanned helicopter. *Biosystems Engineering, 90*, 369–379.

Verhoef, W. (1984). Light scattering by leaf layers with application to canopy reflectance modeling: the SAIL model. *Remote Sensing of Environment, 16*, 125–141.

Weltzien, H. C. (1981). Geographical distribution of downy mildews. In D. M. Spencer (Ed.), *The downy mildews* (pp. 31–43). London: Academic Press.

West, J. S., Bravo, C., Oberti, R., Lemaire, D., Moshou, D., & McCartney, H. A. (2003). The potential of optical canopy measurement for targeted control of field crop diseases. *Annual Review of Phytopathology, 41*, 593–614.

Yang, C., Everitt, J. H., Bradford, J. M., & Murden, D. (2009). Comparison of airborne multispectral and hyperspectral imagery for estimating grain sorghum yield. *Transactions of the ASABE, 52*, 641–649.

Yossifovitch, M. (1929). *Peronospora arborescens* (Berk.) de Bary, parasite très important de *Papaver somniferum* en Yougoslavie (*Peronospora arborescens* (Berk.) de Bary, very important parasite of

Papaver somniferum in Yugoslavia). *Revue de Pathologie et d'Entomologie en Agriculture, 16*, 235–270.

Zaitseva, V. A., Lovchikova, L. P., Naumenko, E. K., Kononovich, S. I., Nikonenko, S. V., & Plyuta, V. E. (1997). Brightness coefficients of opium poppy crops and particular phytoelements of the poppy in various vegetative stages. *Journal of Applied Spectroscopy, 64*, 88–93.

Zarco-Tejada, P. J., Berjón, A., López-Lozano, R., Miller, J. R., Martín, P., Cachorro, V., et al. (2005). Assessing vineyard condition with hyperspectral indices: leaf & canopy reflectance simulation in a rowstructured discontinuous canopy. *Remote Sensing of Environment, 99*, 271–287.

Zarco-Tejada, P. J., Berni, J. A. J., Suárez, L., & Fereres, E. (2008). A new era in remote sensing of crops with unmanned robots. *SPIE Newsroom*. doi:10.1117/2.1200812.1438.

Zarco-Tejada, P. J., González-Dugo, V., & Berni, J. A. J. (2012). Fluorescence, temperature and narrow-band indices acquired from a UAV for water stress detection using a hyperspectral imager and a thermal camera. *Remote Sensing of Environment, 117*, 322–337.